IOP Publishing Journal of Physics D: Applied Physics

J. Phys. D: Appl. Phys. **51** (2018) 133002 (13pp) https://doi.org/10.1088/1361-6463/aaaf08

Topical Review

A review of recent progress in heterogeneous silicon tandem solar cells

Masafumi Yamaguchi, Kan-Hua Lee[1], Kenji Araki and Nobuaki Kojima

Toyota Technological Institute, Hisakata 2-12-1, Tempaku-ku, Nagoya, Japan

E-mail: kanhua@toyota-ti.ac.jp and masafumi@toyota-ti.ac.jp

Received 23 June 2017, revised 6 February 2018
Accepted for publication 13 February 2018
Published 2 March 2018

Abstract

Silicon solar cells are the most established solar cell technology and are expected to dominate the market in the near future. As state-of-the-art silicon solar cells are approaching the Shockley–Queisser limit, stacking silicon solar cells with other photovoltaic materials to form multi-junction devices is an obvious pathway to further raise the efficiency. However, many challenges stand in the way of fully realizing the potential of silicon tandem solar cells because heterogeneously integrating silicon with other materials often degrades their qualities. Recently, above or near 30% silicon tandem solar cell has been demonstrated, showing the promise of achieving high-efficiency and low-cost solar cells via silicon tandem. This paper reviews the recent progress of integrating solar cell with other mainstream solar cell materials. The first part of this review focuses on the integration of silicon with III–V semiconductor solar cells, which is a long-researched topic since the emergence of III–V semiconductors. We will describe the main approaches—heteroepitaxy, wafer bonding and mechanical stacking—as well as other novel approaches. The second part introduces the integration of silicon with polycrystalline thin-film solar cells, mainly perovskites on silicon solar cells because of its rapid progress recently. We will also use an analytical model to compare the material qualities of different types of silicon tandem solar cells and project their practical efficiency limits.

Keywords: solar cells, Si tandem, III–V compounds, II–VI compounds, chalcopyrite, perovskite

(Some figures may appear in colour only in the online journal)

1. Introduction

To achieve a sustainable energy future, solar electricity and solar thermal generation have to increase its share of global energy to 20% in 2050 and 70% in 2100, as projected by the German Advisory Council on Global Change [1]. As the 'engine' of the solar electricity conversion, the solar cell has to be more efficient and cheaper in order to realize this scenario.

Silicon solar cells are by far the most dominant solar cell material in the photovoltaic (PV) market and are expected to stay dominant in the near future for several reasons. Firstly, the technology of manufacturing silicon solar cells is very mature and keeps advancing. State-of-the-art silicon solar cells can achieve more than 25% efficiency. In the meantime, the areal manufacturing cost of silicon solar cells keeps reducing and is closing its gap to the areal cost of other low-temperature deposited thin film solar cells. Secondly, silicon has been proven to be very reliable and meets the lifetime requirement of most PV applications. Thirdly, silicon is an earth-abundant element, making it free from the shortage of supply of raw materials.

The conversion efficiencies of mainstream solar cell materials were dramatically improved in the last few decades, but they are also converging to their limits. Figure 1 presents the historical record-efficiency of various types of solar cells along with their extrapolations. This analysis was originally

[1] The contributions of the first, second author are equal.

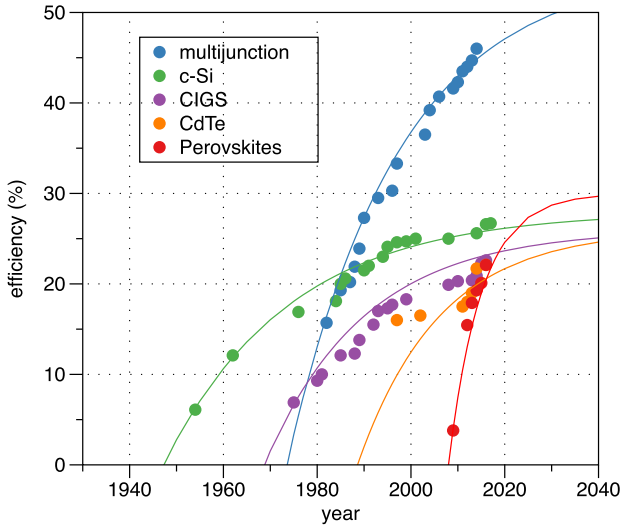

Figure 1. Record efficiencies of III–V multi-junction, crystalline silicon, copper indium gallium diselenide (CIGS), cadmium telluride (CdTe) and perovskite solar cells. Solid lines are the fitted trajectories using the exponential regression model proposed in [2]. Reprinted from [2], Copyright © 2002, with permission from Elsevier. All rights reserved.

presented in [2]. These curves were fitted by only the historical data and assumed that the advances of each technology is largely progressive rather than disruptive. The extrapolations show that the progress of the efficiencies are converging or will converge soon, which is mainly bounded by the Shockley–Queisser limit.

An important strategy to raise the efficiency of solar cells is stacking solar cell materials with different bandgaps to absorb different colors of the solar spectrum. This so-called 'multi-junction' approach can reduce the thermalization loss due a high-energy photon absorbed by a small-bandgap material, and below-band-gap loss due to a low-energy photon failed to excite a high-bandgap material. This concept was most successfully implemented in a III–V compound semiconductor solar cell, since a compound semiconductor has a good range of lattice parameters and bandgaps to choose from. Thanks to the maturity of the III–V semiconductor industry, high quality III–V materials can be fabricated. Three-junction (3J) GaInP/InGaAs/Ge solar cell can achieve more than 40% efficiency under 500 suns. The world-record efficiency of a 3J cell comprises of lattice-mismatched GaInP, 1.42 eV-InGaAs and 1.0 eV-InGaAs, which can reach 44.4% efficiency under 302 suns, whereas a four-junction (4J) GaInP/GaAs;GaInAsP/GaInAs could reach 46.0% at 508 suns [3].

Despite its superior performance, a III–V solar cell has a very small market share in solar electricity generation because of its high manufacturing cost. III–V solar cells are only adopted by the systems in which the cost of solar cells takes only a very small portion, such as satellites or high-concentration photovoltaic systems. Replacing the epitaxial growth substrate by silicon is a promising pathway to reduce the manufacturing cost.

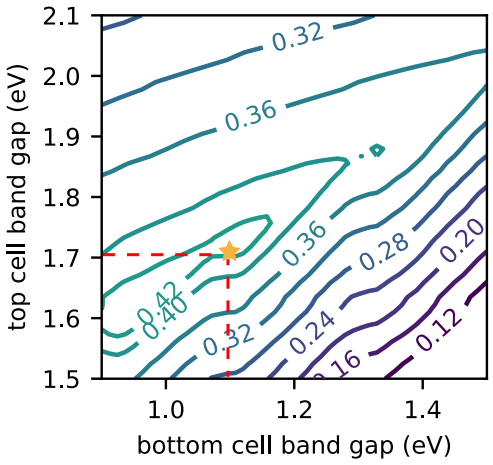

Figure 2. Efficiency contours of 2J tandem solar cells against the bandgaps at Shockley–Queisser limit.

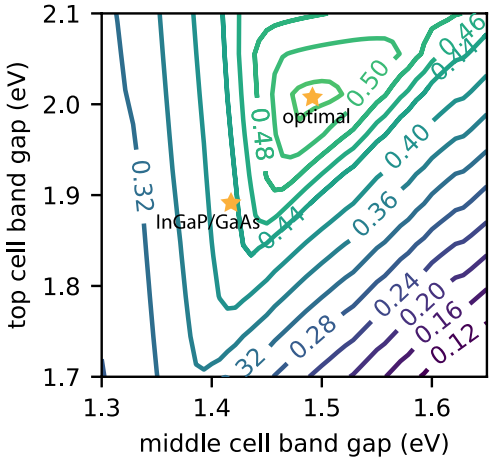

Figure 3. Efficiency contours of 3J solar cells against top and middle cell's bandgaps with silicon bottom cell.

From the viewpoint of other solar cell materials, stacking them on a silicon cell to make two or more junction solar cells provides a way to fundamentally improve their limits of conversion efficiencies. Since these materials generally have a higher bandgap than silicon, adding a silicon cell can essentially extend their absorption edge towards lower-wavelength part of the solar spectrum.

This paper reviews the latest development of heterogeneous silicon tandem solar cells. Our focus will be all potential top cell materials other than silicon, leaving the review of all-silicon multi-junction technology elsewhere [4]. We will first give an overview of the general design consideration and cell configurations of silicon tandem solar cells. After that, we review the recent progress of different types of silicon tandem solar cells, highlighting the advantages and scientific challenges of each approach. Finally, we introduce a simple analytical model to summarize the present status of silicon tandem cells and their efficiency prospects. For brevity, the reported characteristic results of solar cells were all measured under standard test conditions (AM1.5g spectrum normalized to 1000 W m^{-2}, tested at 25 °C) unless otherwise stated.

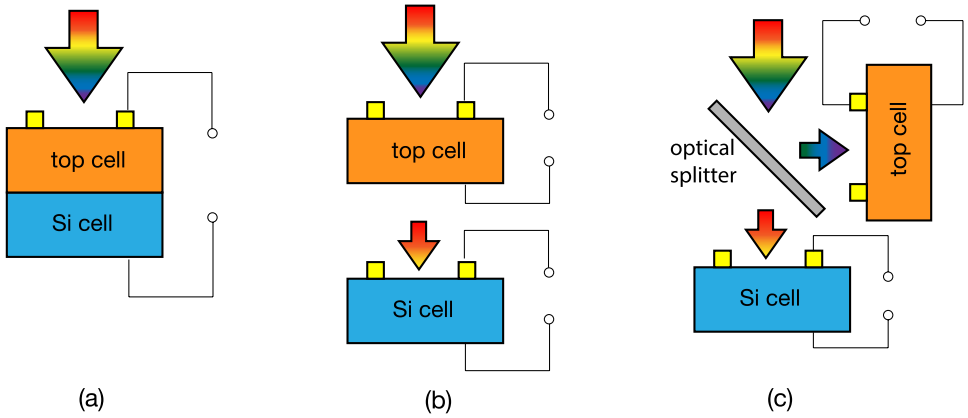

Figure 4. An illustration of three main tandem solar cell architectures. Reproduced with permission from [8]. (a) Two-terminal, (b) mechanically-stacked four-terminal, (c) optical splitting.

2. Design consideration and challenges of silicon tandem solar cells

Bandgap combination is one of the most important considerations when designing tandem solar cells. Figure 2 presents the efficiency contours of two-junction (2J) solar cells against top and bottom cell bandgaps [5, 6, 7]. The optimal bandgap combination of a 2J device is around 1.62 eV and 0.91 eV, which gives a limiting efficiency of 42.8%. Constraining the bottom cell to the bandgap of silicon (1.1 eV) gives a maximum limiting efficiency of 42.4% with a 1.72 eV top cell, which is close to the efficiency of optimal bandgap combination. In the case of 3J tandem devices with silicon bottom cells, the optimal bandgap combination of top and middle cell is 2.01 eV and 1.5 eV. The efficiency contours of the 3J silicon tandem cell versus the top and middle cell bandgaps are plotted in figure 3. This combination deviates from the commonly used GaInP(1.87eV)/InGaAs(1.42eV) in III–V multi-junction solar cells. At present, since high quality solar cell materials of any type with bandgaps of 2.01 eV and 1.5 eV are difficult to fabricate, using GaInP(1.87eV)/InGaAs(1.42eV) as the top junctions on silicon is a good alternative.

There are three major ways to integrate silicon with other materials to implement a multi-junction device, which are illustrated in figure 4. The first one is two-terminal, series-connected configuration, in which the subcells are connected by conductive layers that can transport the carrier from one subcell to another. The tandem device will then only have two terminals and can be simply operated as a standard single junction solar cell, which greatly simplifies its integration in a PV module and system. However, since the subcells are connected in series, the requirement of current-match reduces the choices of materials in terms of bandgaps. In addition, the fabrication of highly conductive and optically-transparent conductive layers between each subcell is also challenging. The second configuration is mechanical stacked tandem device, in which the subcells are also vertically stacked but each subcell has its own terminals to be operated individually to their own maximum power points. Compared with the two-terminal tandem configuration, this approach relieves the requirement of current-match and a conductive layer between subcells, but it incurs other costs in modules and systems, such as cables and inverters. The third approach is using an optical spectrum splitter to redirect the different colors of the solar spectrum to each subcell. The subcells are just operated individually without any integration. The choice of subcells is then very flexible. This configuration transfers the difficulty from the cell integration to the designs of the PV module. Our review will only focus on the first two configurations because the third approach is beyond the scope of solar cell fabrication.

3. III–V semiconductor solar cells on silicon

Integrating III–V compound semiconductors with silicon substrates has been studied extensively because it is a promising way to significantly reduce the cost of III–V semiconductor devices. The main challenge comes from the lattice mismatch between silicon and the commonly used III–V compound semiconductors. Monolithically epitaxial grown III–V multi-junction cells typically need all the epitaxial layers to have the same lattice constant to maintain high crystallinity, which is essential to attain high efficiency. Figure 5 shows the bandgaps versus lattice constants of commonly used III–V compound semiconductor versus their lattice constants. As shown in this figure, the choices of III–V compounds latticed match to silicon is very limited. Commercial GaInP/GaAs/Ge 3J solar cells composed of epitaxial layers lattice-matched to GaAs. Most of the research efforts that aim to achieve more junctions are also based on this material system.

The problem of lattice mismatch is aggravated by the difference of thermal expansion coefficients between III–V semiconductors and silicon. The epitaxial process is usually needed to heat up the substrate to a few hundred degrees Celsius and then cool down to room temperature. This results in bowing, bending or cracking in the III–V on silicon wafers. The thermal expansion coefficients of III–V semiconductors typically range from 4.7×10^{-6} K^{-1} to 5.7×10^{-6} K^{-1}, whereas the thermal expansion coefficients of silicon is 2.6×10^{-6} K^{-1}. As a result, even with lattice-matched growth, e.g. GaP on silicon, strain is introduced in the III–V layer during the cooling down of the sample.

Notable III–V/Si solar cell results are mainly achieved by on-silicon-heterepitaxy, wafer bonding and mechanical stacking, which will be described in this section. We will also

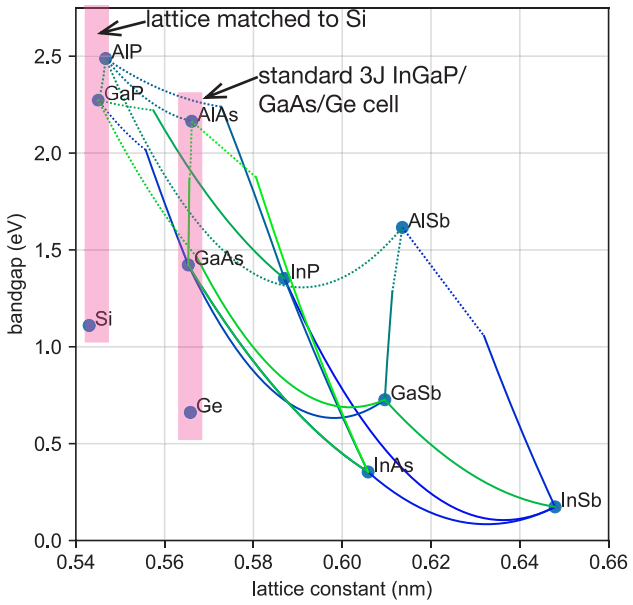

Figure 5. Bandgaps against lattice constants of silicon, germanium and III–V semiconductors, based on the material parameters presented in [9].

review some novel approaches that could potentially address the issue of lattice mismatch. The results of these III-V/Si devices are listed in table 1.

3.1. Direct heteroepitaxy of III–V semiconductors on silicon

It has been demonstrated that III–V semiconductors can be directly grown on silicon substrates without buffer layers despite of the lattice mismatch between III–V and silicon. Direct heteroepitaxy of III–V materials on silicon typically starts with a two-step process [10]: the first 10 nm thick GaAs layer was grown at low temperature (∼400 °C) to enhance the nucleation. Then, the temperature is ramped up to around 600 °C–750 °C to obtain better uniformity of the epitaxial layer. After this initial growth, either or both thermal cycle annealing (TCA) and strained-layer super lattices (SLSs) can be used to manipulate the stress in the lattices during the growth to reduce the defect density.

TCA was carried out by cycling the substrate temperature between the growth temperature (700 °C–900 °C) and room temperature [11, 12]. Due to the mismatch of the thermal expansion coefficients between III–V and silicon, TCA could increase the movement of dislocations and reduce the stress in the crystal, resulting in the reduction of dislocation densities. Yamaguchi *et al* [11] presented an empirical model that uses reaction rate equations to analyze the annihilation and coalescence of defects during the thermal cycle processes. This work compared several GaAs-on-Si samples grown by different thermal cycle annealing conditions. Then, the defect density was observed by transmission electron microscopy and etch-pit density counting after molten KOH etching. It was found that the etch-pit density can be reduced to less than 2×10^6 cm^{-2}. The analytical model suggests that this is mainly caused by the relaxation of thermal stress.

Inserting repeating SLS structure after TCA can further decrease the dislocation defects by relieving the strain between GaAs and silicon. Layer structures such as $In_{0.1}Ga_{0.9}As$/GaAs, $In_{0.1}Ga_{0.9}As$/$GaAs_{0.8}P_{0.2}$ and $Al_{0.6}Ga_{0.4}As$/GaAs have been attempted for GaAs on silicon growth [13–15]. This methodology was also used to investigate the reduction of defect density due to SLS insertion [15]. This study found that the dislocation density can be reduced to 1×10^6 cm^{-2} and can potentially be further reduced by increasing the thickness of individual superlattice layers. The reduction of dislocation density can be described by the model presented in [16].

The authors have demonstrated GaAs solar cell grown on silicon substrate with 18.3% efficiency at AM0 and 20% at AM1.5 [17]. In addition, high quality AlGaAs film grown on silicon substrates using TCA was reported in [18, 19].

3.2. Heteroepitaxy growth with buffer layer

At present, much of the attention was turned to using graded buffer layers to transfer the lattice constants of silicon to that of III–V materials. Materials with the same or nearly same lattice constant to silicon is initially grown on silicon substrates and its composition is gradually changed to match the lattice constant of the desired III–V materials. In this section, we review two of the most successful graded buffer layers, Si_xGe_{1-x} and $GaAs_yP_{1-y}$.

3.2.1. Graded Si_xGe_{1-x} buffer Since the epitaxial growth of III–V multi-junction solar cells on germanium substrates is very well-established, using SiGe to bridge the lattice constant from silicon to germanium is a natural choice. The research group in MIT demonstrated that utilizing chemical mechanical polishing half-way between the growth of SiGe can lower the threading dislocation density to ∼10^6 cm^{-2} [20]. After that, Andre *et al* demonstrated a 18.1% 1J GaAs solar cell by using technique [21]. The same team later demonstrated a high open-circuit voltage 2J GaInP/GaAs cell on SiGe/Si [22], showing the promise of achieving high efficiency cells using this approach.

Low bandgap and thick layers (typically 10 μm) of SiGe make it absorb most of the photons before they reach the bottom silicon, so the bottom silicon can only be used as an inactive substrate instead of an activated cell. A compromise is to use active SiGe as the bottom cell and GaAsP as its top cell to implement a bandgap combination close to GaAsP/Si. This GaAsP/SiGe dual-junction device was demonstrated in [23–28].

3.2.2. Graded $GaAs_yP_{1-y}$ buffer Gallium phosphide (GaP) is the most obvious choice of the III–V material for direct heteroepitaxy on silicon substrates because of its close match of lattice parameter against silicon, as in shown in figure 5. By gradually adding the fraction of arsenic to form ternary $GaAs_yP_{1-y}$, the lattice parameters can be increased to match the III–V compounds of desired bandgaps.

With this buffer layer, a natural choice of the top cells is 1.7 eV GaAsP for a 2J device and GaInP(2.01eV)/GaAsP(1.5eV) for a 3J device. These are the optimal bandgaps for silicon bottom cells, as discussed in the previous section. Despite the close match of lattice parameters between GaP and silicon, growing high quality GaP on silicon is not

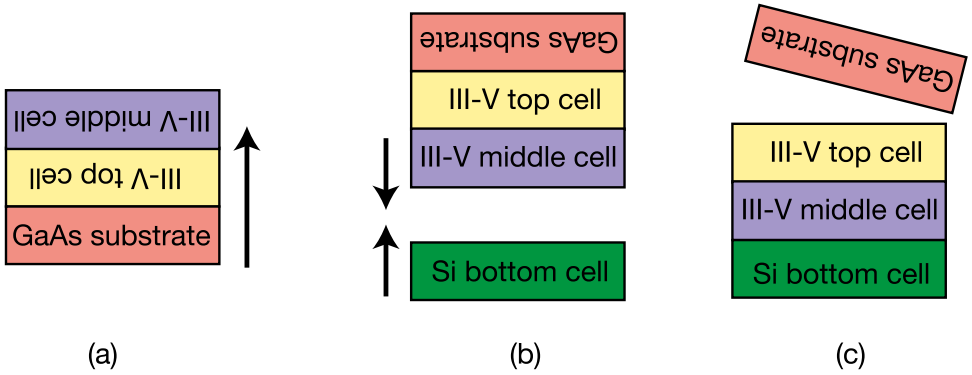

Figure 6. An illustration of the workflow of the wafer bonding process. (a) III-V epitaxial growth, (b) wafer bonding, (c) GaAs wafer lift-off.

a straightforward task. Growing polar GaP on a pristine non-polar silicon substrate causes many nucleation-related issues, such as anti-phase domains, stacking faults and dislocations. These issues has been overcome by choosing an appropriate index and orientation of the substrate as well as nucleating the inter-surfaces with specific procedures [29, 30]. Lee's research group at UIUC has recently demonstrated a 15.3%-efficiency, single-junction $GaAs_{0.76}P_{0.24}$ molecular-beam-epitaxy(MBE)-grown solar cell on a GaP/Si template, which is the highest efficiency solar cell of its kind [31]. The threading dislocation density in the buffer layer was lowered to 5.3×10^6 cm^{-2}, built upon their previous work on controlling this defect [32].

Fabricating high-quality tunnel junctions is another challenge to implement 2J GaAsP/Si or GaInP/GaAsP/Si solar cells. Chmielewski *et al* demonstrated $GaAs_{0.9}P_{0.1}$ tunnel diodes that are grown on a GaAs substrate [33]. With some adjustment of this tunnel junction design, this research group demonstrated the preliminary results of dual-junction GaAsP//Si solar cells by both MBE and metal-organic chemical vapor deposition (MOCVD) [34].

Another alternative is to increase the lattice constant to match that of GaAs. This approach introduces larger lattice mismatch and deviates the bandgaps of the top cells from optimal values, but a better quality of top cells can be obtained in return. Dimroth *et al* demonstrated a 16.4% efficiency GaInP/GaAs dual-junction solar cell [35] grown on silicon, against the 27.1% control cell that was grown on a GaAs substrate. The efficiency loss largely comes from the high threading dislocation density (>10^8 cm^{-2}). In addition, the authors reported that no indications of cracking due to thermal expansion coefficient mismatch were found in the devices grown heteroepitaxy on silicon.

3.3. Wafer bonding

Direct wafer bonding is an established technique in optoelectronics and integrated circuit industry for covalently bonding together different material. This approach can integrate wafers with different lattice constants without causing much dislocation defects. Also, since the bonding layers between two wafers are very thin, parasitic resistance and optical loss are much smaller compared to the buffer layer used in heteroepitaxy. The typical workflow of making wafer-bonded III–V on a silicon device is illustrated in figure 6. The III–V layers is grown on a III–V substrate as usual. After that, the epitaxial wafer is bonded onto silicon, followed by the removal of the III–V substrate. Since III–V solar cells were firstly grown on a III–V wafer, being able to reuse the III–V wafer as many times as possible is another challenge in order to make this process economically viable.

In general, direct wafer bonding (figure 6(b)) includes three steps: (1) wafer preprocessing, (2) pre-bonding the wafers by mechanical compression and (3) post-annealing the wafers to form strong bonds. Two of the wafer preprocessing approaches are the most successful in fabricating high-performance multi-junction solar cells. The first one uses wet-chemical etching to a hydrogen-terminated surface and brings together the wafer via hydrogen bonds. Post-anneal then desorp the hydrogen and form the covalent bonds in the interface [36]. This method is often referred to as fusion bonding. The second one uses plasma or a fast argon atom beam to activate the surfaces of each wafer prior to the bonding process, which is often referred to as surface-activated bonding (SAB). This approach lowers the bonding energy and makes post-annealing no longer essential [37]. Although the post-annealing process could strengthen the bonds between the wafer and results in electrical properties, it also damages the wafer due to the differences of thermal expansion coefficients between the two wafers.

Both of these approaches have been applied to fabricate high-efficiency four- or five-junction solar cells [38–40]. Most of the wafer-bonded III–V/Si multi-junction solar cells were implemented by SAB because they do not require post-annealing. Electrical properties of the wafer interface bonded by SAB was reported in [41].

Wafer-bonded triple-junction GaInP/GaAs/Si solar cells were firstly demonstrated by Fraunhofer ISE [42]. The process was kept optimized, including replacing the middle cell by AlGaAs to give better current match [43]. Recently, Fhg-ISE demonstrated a 31.3%-efficiency two-terminal 3J GaInP/GaAs/Si cell with 3.98 cm^2 area by using a surface activated bonding technique [44]. Osaka City University also demonstrated a 25.5%-one-sun-efficiency GaInP/GaAs/Si 3-junction solar cell with 0.25 cm^2 area by using SAB [45]. A III–V/Si device integrated by direct fusion bonding was also demonstrated in [46].

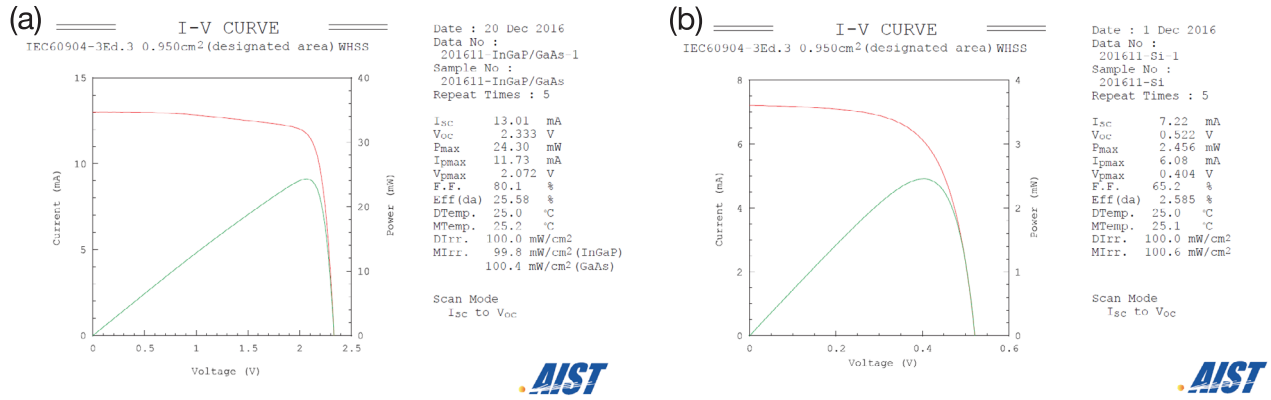

Figure 7. Current-voltage characteristics of the (a) GaInP/GaAs top cell and (b) crystalline silicon bottom cell in the mechanical-stacked GaInP/GaAs//Si 3J solar cell. The top cell is the same as the one presented in [47], and the bottom cell is recently fabricated.

Table 1. Notable results for III–V/Si tandem solar cells. In the 'Cell' column, integration of III–V with active silicon junctions is denoted by a double slash //, whereas integration of III–V on inactive silicon substrates is denoted by a single slash /. The figures of merit of the subcells in a four-terminal (4T) device are denoted as (top cell's value)//(bottom cell's value). All the solar cells were reported to be characterized under the AM1.5g spectrum unless otherwise footnoted.

#	Cell	Efficiency	Area (cm^2)	Voc (V)	Jsc (mA cm^{-2})	FF	Interconnect	Note
S1	GaAs/Si(1J)	20.1	1	0.93	27.0	80.0	heteroepitaxy	TTI *et al* [17]
S2	GaAs/Si(1J)	18.3[a]	1	0.94	33.2	79.1	heteroepitaxy	TTI *et al* [17]
S3	AlGaAs/Si(2J)	21.2[a]	N/A	1.57	23.6	77.2	heteroepitaxy	NIT, 1996 [19]
S4	GaAs//Si(2J)	25.2	1.0	1.55	27.9	58.0	wafer bonding	UTokyo, 2012 [46]
S5	GaInP/GaAs/Si(2J)	16.4	4.0	2.45	11.2	75.3	heteroepitaxy	Fhg-ISE, 2014 [35]
S6	GaInP/GaAs/Si(2J)	26.0	4	2.385	12.7	85.9	wafer bonding	Fhg-ISE, 2014 [35]
S7	GaInP/GaAs//Si(3J)	27.9[b]	0.054	3.335	483	82.6	wafer bonding	Fhg-ISE, 2013 [76]
S8	GaInP/GaAs//Si(3J)	25.5	0.64	2.74	11.8	79.0	metal interconnect	McMaster, 2014 [56]
S9	GaAsP//Si(2J)	12.9	0.04	1.62	10.2	79.5	heteroepitaxy	OSU, 2016 [34]
S10	GaAs-NW//Si(2J)	11.4	0.01	0.96	20.6	57.8	nanowires	USC [68]
S11	GaInP/GaAs//Si(3J)	25.5	0.25	2.847	10.94	81.83	wafer bonding	OCU[c], 2015 [45]
S12	GaInP/GaAs//Si(3J)	23.2	0.1448	2.81	10.46	79.0	PdNP array	AIST, 2016 [55]
S13	GaInP//Si(2J)	29.8 (18.1//11.7)	1.0	1.456// 0.667	14.15 22.7	87.9 76.2	4T by epoxy	NREL, 2016 [49]
S14	GaInP/GaAs//Si(3J)	30.2	3.963	3.046	11.9	83.0	wafer bonding	Fhg-ISE, 2017 [43]
S15	GaAsP/Si(1J)	12.0	0.1	1.15	13.3	79.0	heteroepitaxy	Yale/UIUC, 2016 [32]
S16	GaInP/GaAs//Si(3J)	28.6//4.4	3.604	2.446// 0.694	13.9// 8.3	84.7// 76.6	epoxy	Sharp, 2016 [51]
S17	GaInP/GaAs//Si(3J)	31.3	3.98	3.046	11.7	87.5	wafer bonding	Fhg-ISE, 2017 [44]
S18	GaInP/GaAs//Si(3J)	35.91 30.01//5.9	1.00	2.520// 0.681	13.61// 22.03	87.5// 78.5	4T by epoxy	EPFL *et al* 2017 [50]
S19	GaAs//Si(2J)	32.82 26.83//5.99	1.00	1.092// 0.6828	28.9// 11.07	85.0// 79.2	4T by epoxy	EPFL *et al*, 2017 [50]
S20	GaInP/GaAs//Si(3J)	28.1 25.58//2.585	0.95	2.33// 0.52	13.70// 7.6	80.1// 65.2	4T	TTI *et al*,2017 [47] and this work

[a] Measured under AM0 (1353 W m^{-2})
[b] Measured under AM1.5d at 48.3 suns.
[c] Osaka City University.

3.4. Mechanical stack

Mechanical stacked III–V/Si solar cells use adhesive materials to stack III–V and silicon solar cells. This approach prevents the lattice dislocation defects caused by forming the chemical bonds of III–V and silicon, as we described in sections 3.1, 3.2 and 3.3. However, if the adhesive material is electrically insulated, the III–V and silicon subcell need their own terminals instead of being connected. This four-terminal solar cell would incur an extra cost in making the PV modules. Takamoto *et al* reports one of the early efforts of mechanical-stack solar cells in [47]. The III–V solar cell reported in this work along with an upgraded silicon bottom cell have a combined efficiency of 28.16%, as verified by AIST. The I-V characteristic results were presented in figure 7. A series of papers report the joint research efforts of mechanically-stacked III–V//Si cells by NREL, EPFL and CSEM [48] [49]. This culminates in the

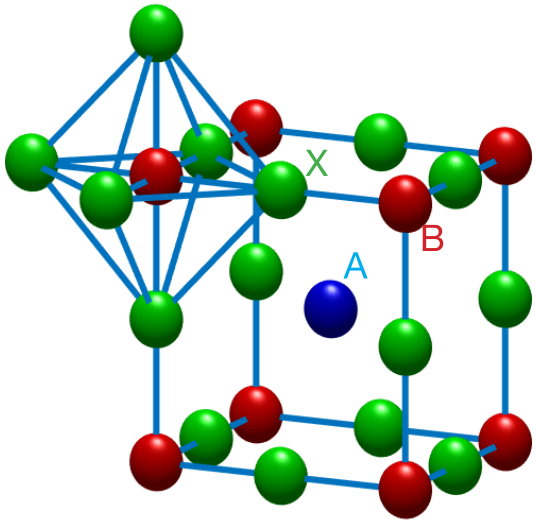

Figure 8. The lattice structure of ABX_3. The A cation occupies a cubo-octahedral site where as the B cation occupies an octahedral site (BX_6).

demonstration of a 32.8% 2J GaAs//Si and a 35.9% 3J GaInP/GaAs//Si III–V//Si solar cells reported in [3, 50]. A 32.45% 2J GaInP//Si 2J cell was also demonstrated in the same paper. In this work, all the III–V subcells were grown by MOCVD and its epitaxial substrate was removed after the subcells were transferred to a glass substrate. A silicon heterojunction (SHJ) bottom cell was attached to the other side of the same glass substrate. Lifting off epitaxial substrates not only reduces the parasitic absorption loss, but also offers a pathway of cost reduction by reusing the substrate.

The Sharp Corporation has also achieved 33.0% efficiency with 3.604 cm^2 area GaInP/GaAs//Si 3J solar cells by using mechanical stack [51].

AIST demonstrated a novel interconnect layer made of palladium nanoparticle (PdNP) arrays between III–V and silicon that could be both optically transparent and electrical conductive, allowing two-terminal configuration for mechanical stack cells. The PdNP array makes use of van der Waals bonding to stack III–V an silicon subcells [52]. Details of the fabrication are described in [53, 54]. The averaged size of PdNP is 37 nm and the pitch of the array is 95 nm. This leads to a PdNP density of 1.3×10^{10} cm^{-2} and a surface coverage ratio of 12%. A 23.2%-efficiency under 1-sun with GaInP/GaAs/Si 3-junction solar cell was fabricated by using PdNP array-mediated bonding [55].

A research group at McMaster University demonstrated a two-terminal mechanical stack III–V/Si cell using direct metal interconnect [56]. In this work, both sides of the III–V and silicon solar cells were deposited with metal contacts and then bonded by transparent epoxy. The III–V and Si subcells are electrically connected by these metal contacts. A 25.5%-efficiency GaInP/GaAs/Si 3J solar cell is achieved with this approach.

3.5. III–V nanowires and selective area growth

Nanowires (NWs) generally refer to nanostructures with a diameter of the order of nanometers and width-to-length ratio more than 1000. An array of NWs can greatly enhance the light trapping and thus increase the absorption compared to conventional solar cells [57, 58]. Semiconductor NW solar cells have been developed rapidly in the last decade [59, 60]. 13.8%- and 15.3%-efficiency has been achieved by using InP and GaAs NWs [61, 62]. Since the strain induced lattice-mismatch could be relaxed in the sidewall of NWs [63–66], growing III–V NWs on silicon is a promising alternative to implement multi-junction solar cells [67]. The optimal bandgap of III–V NWs grown on silicon substrates is the same as bulk materials discussed in section 2. Recently, Yao *et al* [68] demonstrated a selective area grown GaAs n-i-p NW array on top of a Si cell and a total efficiency of 11.4% . The top GaAs NW solar cell has a p+ emitter, undoped segment, n-type base, and n+ root for the connecting junction with p+ Si. The bottom silicon solar cell has a p+ emitter, n-type base, and n+ back surface field. The NWs are embedded in transparent insulating polymer benzocyclobutene. The top contact is indium tin oxide (ITO) and the back contact is aluminum. Although it has been demonstrated that NW solar cells can achieve a very high photocurrent, their low Voc indicates strong recombination loss in the surfaces and interfaces in the NWs, which is the most pressing challenge to improve the efficiencies of NW solar cells.

Selective area growth uses nanostructures patterned on silicon substrates to reduce the lattice-mismatch-induced strain [69]. This field has already attracted large amounts of attention and research efforts [70–72]. Typically, dielectric, nanometer-sized materials such as SiO_2 are patterned on silicon substrates by electron-beam lithography [73] or nanoimprint [74]. Greenway *et al* demonstrated a GaAs-on-Si device with a short-circuit current of 9.7 mA cm^{-2} using this approach [75]. However, no fully functional III–V-on-Si device has been publicly demonstrated yet.

4. Polycrystalline thin-film solar cells on silicon

Unlike monocrystalline III–V or silicon, high defect tolerance of some polycrystalline or amorphous semiconductor solar cells [77] make them less demanding on the material quality and cheaper to make. Materials such as cadmium telluride (CdTe), copper indium gallium diselenide and perovskites belong to this category. The main motivation of integrating these materials with silicon is to extend the absorption edge towards longer wavelengths. Since these materials have a higher tolerance on defects, lattice mismatch is not a major concern for them to deposit on silicon solar cells. However, not all of these materials can be deposited on silicon substrates with reasonable quality. At present, only a-Si, CdTe, perovskites integrated silicon are successfully demonstrated. Since the focus of this review paper is heterogeneous material integration with silicon, we will only review the recent progress of chalcogenide and perovskite solar cells.

4.1. Perovskite on silicon

Perovskite generally refers to crystals with a structure of ABX_3 formula, where X is oxygen or halogen. The larger A cation sits on a cubo-octahedral site surrounded by twelve X anions

Table 2. Notable results for perovskite/Si tandem solar cells. The figures of merit of the subcells in a four-terminal device are denoted as (top cell's value)//(bottom cell's value). All the solar cells were reported to be characterized under AM1.5g spectrum.

#	Efficiency	Area (cm^2)	Voc (V)	Jsc (mA cm^{-2})	FF	Interconnect	Note
P1	13.4(6.2//7.2)	0.2773	0.821//0.689	18.5//13.7	67.0//76.7	4T	EPFL *et al*, 2014 [86]
P2	12.4//4.3	0.12–0.39	1.025//0.547	17.5//11.1	71.0//70.4	4T	Stanford *et al*, 2014 [87]
P3	13.7	1	1	11.5	0.75	Si TJ[a]	MIT and Stanford [88]
P4	19.1	0.27	1.759	14	77.3	ITO	HZB *et al* [89]
P5	21.2	0.17	1.692	15.8	79.9	IZO	EPFL *et al* [90]
P6	17.1//7.3	0.715	1.2//0.69	19.4//13.9	75.1//76.4	4T	Oxford [91]
P7	16.6//6.5	0.075	1.08//0.679	20.6//12.3	74.1//77.9	4T	UNL and ASU [92]
P8	20.6	1.43	1.717	16.4	73.1	ITO	EPFL [93]
P9	16.3//8.8	0.25	1.069//0.693	20.1//15.98	76.1//79.5	4T	EPFL [93]
P10	23.6	1	1.65	18.1	79	ITO	Stanford *et al* [83]

[a] Silicon tunnel junction.

Table 3. Candidates of chalcogenide compounds for the top junctions of multi-junction solar cells with silicon bottom cells.

	Top cell of 2J	Top and middle cell of 3J
III–V	GaInP	(Al)GaInP/InGa(As)P
	(Al)GaAs	(Al)GaInP/AlGaAs
		GaPN/GaAsPN
II–VI	CdSe	CdZnTe/Cd(Se)Te
	CdZnTe	CdZnSeTe/Cd(Se)Te
	CdMnTe	CdMnTe/Cd(Se)Te
		CdSe/Cd(Se)Te
I-III–VI_2	$CuGaSe_2$	$Cu(In,Ga)(S,Se)_2/CuInS_2$
	$Cu(Al,In)Se_2$	$Cu(In,Ga)(S,Se)_2/Cu(In,Ga)(S,Se)_2$
	$Cu(Al,Ga)Te_2$	$Cu(Al,In)Se_2/Cu(Al,In)Se_2$
	$Ag(Al,In)Se_2$	$Ag(In,Ga)(S,Se)_2/Ag(In,Ga)(S,Se)_2$
	$Ag(Al,Ga)Te_2$	$Cu(Al,Ga)Te_2/Cu(Al,Ga)Te_2$
		$Ag(Al,In)Se_2/Ag(Al,In)Se_2$
		$Ag(Al,Ga)Te_2/Ag(Al,Ga)Te_2$
I_2-II-IV-VI_4	Cu_2ZnGeS_4, $Cu_2ZnGeSe_4$	Cu_2ZnGeS_4/ $Cu_2ZnGeSe_4$
	Cu_2ZnSnS_4	Cu_2ZnGeS_4/ Cu_2ZnSnS_4
II-IV-V_2	$CdGeP_2$, $ZnGe(As,P)_2$,	$ZnGe(As,P)_2/ZnGe(As,P)_2$
	$ZnSi(As,P)_2$, $Cd(Si,Ge)P_2$, $Cd(Ge,Sn)P_2$	$ZnSi(As,P)_2/ZnSi(As,P)_2$

and the smaller B cation sits on anoctahedral site surrounded by six X anions. The crystal structure of perovskite is drawn in figure 8. Halide perovskite material such as $CH_3NH_3PbX_3$ emerges as a prominent candidate for next-generation solar cells because of its strong optical absorption, long diffusion length, tunable bandgap and low-cost processing. Also, like III–V semiconductors, the bandgap of perovskite can be tuned by changing the chemical elements and compositions [78]. Although reliability is still the main issue of perovskite solar cells, nearly 20%-efficiency has been achieved on a device stabilized by 1000 h exposure to one-sun at 50 °C [79]. The history and recent development of perovskite solar cells is reviewed in [80–82]. Replacing the conventional glass substrate by silicon brings the opportunity to further boost efficiencies.

An SHJ cell is typically used as the bottom cell for this purpose, since the amorphous silicon not only passivates the crystalline silicon but also behaves as an interface layer for subsequent deposition of conductive oxides and perovskites. The bandgap of perovskite solar cells is tuned to match the current of silicon bottom cells. The top and bottom junctions are connected by a transparent conductive layer. Ideally, this layer should have small optical loss, high conductivity and reliability. ITO is ubiquitously used in thin-film solar cells as the transparent conductive layer in many types of thin-film solar cells, but the sputtering deposition of ITO raises the concern of damaging the layers underneath. Using a four-terminal configuration could increase the available selection of interconnecting layers.

Table 4. Summary of projected efficiencies (%) of silicon tandem solar cells at different EREs.

	ERE				
Junctions	10^{-5}	10^{-4}	10^{-3}	10^{-2}	10^{-1}
2J	32.5	34.0	35.2	36.5	38.0
3J	35.9	37.5	39.2	40.8	42.5

Successful demonstrations of perovskite/Si solar cells have been reported in a number of publications, which are listed in table 2. We can see that despite the short history of perovskite/Si solar cells, very rapid progress has been achieved in the last

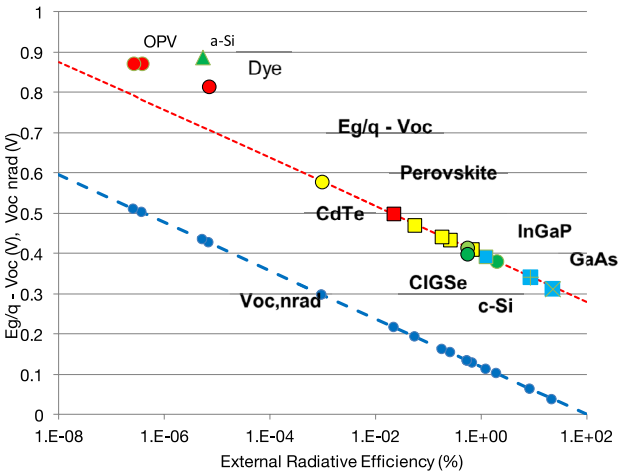

Figure 9. Band-gap-voltage-offset (Eg/q-Voc) and non-radiative Voc (Voc, nrad) in various solar cells as a function of external radiative efficiency (ERE). Reproduced with permission from [100]. Copyright © Materials Research Society 2017.

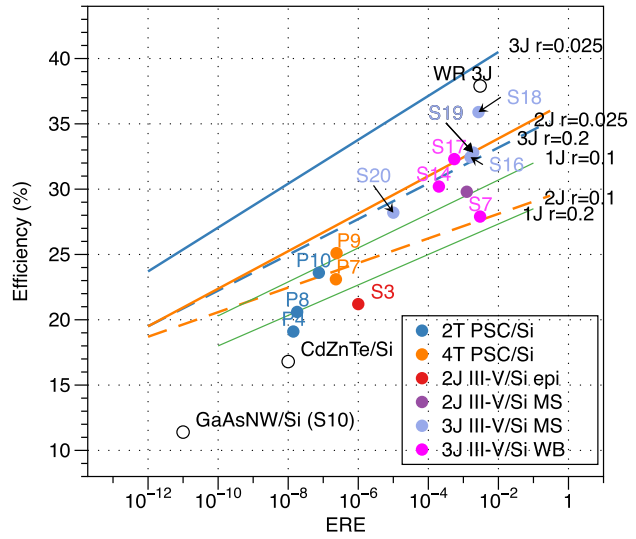

Figure 10. Calculated one-sun efficiencies versus EREs of various junctions and r values (solid and dashed lines), along with selected results of silicon tandem solar cells listed in table 1 and table 2, including two-terminal perovskite/Si (2T PSC/Si), four-terminal perovskite/Si (4T PSC/Si), 2J on-silicon-heteroepitaxy (epi), wafer bonding (WB) and mechanical stack (MS). The current world-record III–V 3J device [3] is added in this plot as a benchmark. The labels of the data points correspond to the row number in table 1 and Table 2.

couple of years. Recently, a two-terminal, 23.6%- efficiency perovskite/Si solar cell with 1 cm^2-area was fabricated and validated by a collaborate effort between Stanford University and Arizona State University [3, 83]. This device has a 1.63 eV-bandgap top cell and a SHJ bottom cell with textured surfaces The two subcells were interconnected by nickel oxide and ITO. The research group in EPFL has recently demonstrated 25.2%- and 23.0%- efficiency, 4-terminal mechanical stacked perovskite/Si 2J tandem cells with an area of 0.25 cm^2 and 1.015 cm^2, respectively.

Much of the efficiency loss of these record-efficiency perovskite/Si solar cells are optical. [84] reported the simulation results of the perovskite/Si solar cell with a layer structure similar to [83] using an empirical one-diode model. The result projects that it is possible to achieve 30-% efficiency by optimizing the layer structure, assuming the diode parameters of each subcell can be maintained as the state-of-the-art cells. A finite difference in time domain simulation reported in [85] also predicts that this solar cell could reach 30-% by employing appropriate light-trapping design. From the point of view of material quality, the ERE of these cells are less than 10^{-6}, which is several order-of-magnitude lower than that of III–V solar cells, as shown in figure 10. This suggests that the material quality of perovskite/Si cells still have large room to improve.

4.2. Chalcogenides on silicon

Integrating chalcogenide solar cells with silicon is proposed as a promising way to reduce their cost per watt [94], but solar cell materials of this kind, including CdTe, chalcopyrites and kesterites, have bandgaps much lower than 1.7 eV. Developing chalcogenide compounds with a higher bandgap is the most pressing issue to implement the silicon tandem cells. Candidates of these compounds are listed in table 3.

To the best of our knowledge, only CdTe on silicon has been publicly demonstrated [95]. In this work, MBE-grown CdZnTe was used as the top cell. This CdZnTe/Si 2J device has an efficiency of 16.8%.

5. Projecting the efficiencies of silicon tandem solar cells

Here, we introduce an analytical model for comparing the sources of efficiency loss of different types of silicon tandem solar cells. This model only attributes the efficiency loss to non-radiative recombination and resistance loss, which is a reasonable assumption because decent solar cells often have very small optical loss. The non-radiative recombination loss is quantified by external radiative efficiency (ERE), which is the ratio of radiatively recombined carriers against all recombined carriers. In other words, we have ERE = 1 at the Shockley–Queisser limit. EREs of state-of-the-art solar cells can be found in a number of publications, such as [6, 96, 97], or [98]. In this work, we estimate the EREs of silicon tandem solar cells by the following relation:

$$V_{oc} = V_{oc,rad} + \frac{kT}{q}\ln(\mathrm{ERE}) \quad (1)$$

where V_{oc} is the measured open-circuit voltage, k is Boltzmann constant, T is the temperature and q is the elementary charge. $V_{oc,rad}$ is the radiative open-circuit voltage. We use $V_{oc,rad}$ values reported in [97] in our analysis. The second term on the right-hand side of equation 1 is denoted as $V_{oc,nrad}$ because it associates to the voltage-loss due to non-radiative recombination. Bandgap-Voc-offset ($Eg/q - V_{oc}$) and $V_{oc,nrad}$ against EREs of state-of-the-art solar cells are plotted in figure 9. The resistance loss of a solar cell is estimated solely from the measured fill factor. The ideal fill factor FF_0, defined as the fill factor without any resistance loss, is estimated by [99]

$$FF_0 = (v_{oc} - \ln(v_{oc} + 0.71))(v_{oc} + 1)^{-1} \quad (2)$$

where v_{oc} is

$$v_{oc} = V_{oc}\,(nkT/q)^{-1}\,. \quad (3)$$

The measured fill factors can then be related to the series resistance and shunt resistance by the following equation [99]:

$$\begin{aligned} FF &\simeq FF_0(1 - r_s)(1 - {r_{sh}}^{-1}) \\ &\simeq FF_0(1 - r_s - {r_{sh}}^{-1}) \\ &= FF_0(1 - r)^{-1} \end{aligned} \quad (4)$$

where r_s is the series resistance and r_{sh} is the shunt resistance normalized to R_{CH}. R_{CH} is defined by [99]

$$R_{CH} = \frac{V_{oc}}{J_{sc}} \quad (5)$$

where r is the total normalized resistance defined by $r = r_s + {r_{sh}}^{-1}$.

By assuming no optical and resistance loss, we can project the efficiency of 2J and 3J silicon tandem solar cell at different EREs, which are listed in table 4. For III–V/Si solar cell, since state-of-the-art III–V top cells can achieve EREs of the order of 10^{-3}, we can expect that the efficiency of III–V/Si achieves 38% if the EREs can be improved by two orders of magnitudes. On the other hand, we expect chalcogenide/Si or perovskite/Si can achieve an efficiency of 35.2%(2J) or 39.2%(3J), assuming that their EREs can be improved to 10^{-3}.

The solid and dashed lines in figure 10 shows the calculated efficiencies against EREs of various values of r using equation 1 to equation 5. The efficiencies and EREs of notable silicon tandem solar cells are also plotted in the same figure for comparison. The values of r were selected so that these lines are close to the reported Si tandem results. We can see that the ERE of the most efficient mechanical stack III–V/Si solar cell(35.9%, [50]) is very close to the current best GaInP/GaAs/InGaAs 3J device, indicating that the degradation of both the III–V and silicon cells due to this integration is manageable. The best wafer-bonded III–V/Si tandem cells [43] can also achieve very high EREs, but the efficiency is lower than the GaInP/GaAs/InGaAs 3J device because the top cell bandgaps in the silicon tandem device is not optimal. III–V/Si tandem solar cells fabricated by direct heteroepitaxy, GaAs-NW/Si and CdZnTe/Si have low efficiencies because their EREs are still far from ideal, and most of the EREs of these cells are already surpassed by those of perovskites/Si solar cells.

6. Conclusions

We surveyed the progress of heterogeneous silicon tandem solar cells and analyzed the prospects of their conversion efficiencies. At present, III–V/Si and perovskites/Si lead the conversion efficiencies of silicon tandem solar cells. Mechanically-stacked and wafer-bonded GaInP/GaAs/Si 3J solar cells can reach more than 30%-efficiency, but these approaches do not really reduce the cost of III–V multijunction solar cells until low-cost wafer-reuse technology is established. Direct heteroepitaxy has the lowest potential cost to integrate III–V and silicon solar cells, but the best demonstrated efficiency struggles to compete with single-junction silicon solar cells. Two-terminal or four-terminal perovskite/Si solar cells have already achieved nearly 24% efficiency. Although this is still lower than the record efficiency of crystalline silicon, perovskite/Si shows great promise because of its rapid developments in the last few years. The development of chalcogenide solar cells on silicon is still preliminary, because fabricating good quality and high bandgap chalcogenide material is still challenging.

Acknowledgments

The authors would like to express sincere thanks to Japan New Energy and Industrial Technology Development Organization (NEDO) for supporting this research (NEDO 15100731-0) for supporting this work, to Prof A Yamamoto, Dr M Sugo, Dr M Tachikawa, Dr T Nishioka, Dr Y Itoh, Dr S Kondo, Dr N Uchida, Dr H Mori, Dr Y Kadota, Prof Y Ohmachi, Dr T Ohhara, previous NTT members, Dr M Imaizumi and Mr S Matsuda, JAXA, and Dr M Al-Jassim and Dr R Ahrienkiel, NREL for their fruitful collaboration and discussion, and to Prof C Ballif and Dr S Essig, EPFL, Dr A Bett and Dr F Dimroth, Fraunhofer-ISE, Prof M Green, UNSW, Prof Y Ohno, Tohoku University, Prof N Shigekwa, Osaka City University, Dr T Takamoto, Sharp, Dr H Tampo, Dr T Ueda, Dr Y Hishikawa, Dr H Mizuno and Dr K Makita, AIST, Dr Y Ichikawa, Tokyo City University and Dr K Yamamoto, Kaneka, for sharing fruitful information with us.

ORCID iDs

Masafumi Yamaguchi https://orcid.org/0000-0002-2825-7217
Kan-Hua Lee https://orcid.org/0000-0001-8560-1515
Kenji Araki https://orcid.org/0000-0002-3216-948X

References

[1] Graßl H, Kokott J, Kulessa M, Luther J, Nuscheler F, Sauerborn R, Schellnhuber H J, Schubert R and Schulze E D 2004 *World in Transition: Towards Sustainable Energy Systems* (London: Earthscan)
[2] Goetzberger A, Luther J and Willeke G 2002 Solar cells: past, present, future *Solar Energy Mater. Solar Cells* **74** 1–11
[3] Green M A, Hishikawa Y, Warta W, Dunlop E D, Levi D H, Hohl-Ebinger J and Ho-Baillie A W H 2017 Solar cell efficiency tables (version 50) *Prog. Photovolt., Res. Appl.* **25** 668–76
[4] Battaglia C, Cuevas A and De Wolf S 2016 High-efficiency crystalline silicon solar cells: status and perspectives *Energy Environ. Sci.* **9** 1552–76
[5] Martí A and Araújo G L 1996 Limiting efficiencies for photovoltaic energy conversion in multigap systems *Solar Energy Mater. Solar Cells* **43** 203–22
[6] Lee K-H, Araki K, Wang L, Kojima N, Ohshita Y and Yamaguchi M 2016 Assessing material qualities and efficiency limits of III–V on silicon solar cells using

external radiative efficiency *Prog. Photovolt., Res. Appl.* **24** 1310–8
[7] Connolly J P, Mencaraglia D, Renard C and Bouchier D 2014 Designing III–V multijunction solar cells on silicon *Prog. Photovolt., Res. Appl.* **22** 810–20
[8] Yamamoto K 2016 26.33% Heterojunction back contact silicon solar cell *The 7th Workshop on Silicon Solar Cells (Busan, November)*
[9] Vurgaftman I, Meyer J R and Ram-Mohan L R 2001 Band parameters for III–V compound semiconductors and their alloys *J. Appl. Phys.* **89** 5815–75
[10] Akiyama M, Kawarada Y and Kaminishi K 1984 Growth of single domain GaAs layer on (100)-oriented Si substrate by MOCVD *Japan. J. Appl. Phys.* **23** L843–5
[11] Yamaguchi M, Yamamoto A, Tachikawa M, Itoh Y and Sugo M 1988 Defect reduction effects in GaAs on Si substrates by thermal annealing *Appl. Phys. Lett.* **53** 2293
[12] Okamoto H, Watanabe Y, Kadota Y and Ohmachi Y 1987 Dislocation reduction in GaAs on Si by thermal cycles and InGaAs/GaAs strained-layer superlattices *Japan. J. Appl. Phys.* **26** L1950–2
[13] Watanabe Y, Kadota Y, Okamoto H, Seki M and Ohmachi Y 1988 Structural properties of GaAs-on-Si with InGaAs/GaAs strained-layer superlattice *J. Cryst. Growth* **93** 459–65
[14] Yamaguchi M, Amano C, Itoh Y, Hane K, Ahrenkiel R K and Al-Jassim M M 1988 Analysis for high-efficiency GaAs solar cells on Si substrates *Record 20th IEEE Photovoltaic Specialists Conf.* vol 1 (IEEE) pp 749–53
[15] Yamaguchi M, Nishioka T and Sugo M 1989 Analysis of strained-layer superlattice effects on dislocation density reduction in GaAs on Si substrates *Appl. Phys. Lett.* **54** 24
[16] Feng Z C and Liu H D 1983 Generalized formula for curvature radius and layer stresses caused by thermal strain in semiconductor multilayer structures *J. Appl. Phys.* **54** 83–5
[17] Yamaguchi M, Ohmachi Y, Oh'hara T, Kadota Y, Imaizumi M and Matsuda S 2001 GaAs solar cells grown on Si substrates for space use *Prog. Photovolt., Res. Appl.* **9** 191–201
[18] Amano C, Sugiura H, Ando K, Yamaguchi M and Saletes A 1987 High-efficiency Al0.3Ga0.7As solar cells grown by molecular beam epitaxy *Appl. Phys. Lett.* **51** 1075–7
[19] Soga T, Kato T, Yang M and Umeno M 1995 High efficiency AlGaAs/Si monolithic tandem solar cell grown by metalorganic chemical vapor deposition *J. Appl. Phys.* **78** 4196–9
[20] Currie M T, Samavedam S B, Langdo T A, Leitz C W and Fitzgerald E A 1998 Controlling threading dislocation densities in Ge on Si using graded SiGe layers and chemical-mechanical polishing *Appl. Phys. Lett.* **72** 1718–20
[21] Andre C L, Carlin J A, Boeckl J J, Wilt D M, Smith M A, Pitera A J, Lee M L, Fitzgerald E A and Ringel S A 2005 Investigations of high-performance GaAs solar cells grown on Ge-$Si_{1-x}Ge_x$-Si substrates *IEEE Trans. Electron Devices* **52** 1055–60
[22] Lueck M R, Andre C L, Pitera A J, Lee M L, Fitzgerald E A and Ringel S A 2006 Dual junction GaInP/GaAs solar cells grown on metamorphic SiGe/Si substrates with high open circuit voltage *IEEE Electron Device Lett.* **27** 142–4
[23] Li D, Zhao X, Wang L, Conrad B, Soeriyadi A, Lochtefeld A, Gerger A, Perez-Wurfl I and Barnett A 2016 Performance improvement for epitaxially grown SiGe on Si solar cell using a compositionally graded SiGe base *Appl. Phys. Lett.* **109** 243503–5
[24] Wang L, Conrad B, Soeriyadi A, Zhao X, Li D, Diaz M, Lochtefeld A, Gerger A, Perez-Wurfl I and Barnett A 2016 Current matched three-terminal dual junction GaAsP/SiGe tandem solar cell on Si *Solar Energy Mater. Solar Cells* **146** 80–6
[25] Zhao X, Li D, Conrad B, Wang L, Soeriyadi A H, Diaz M, Lochtefeld A, Gerger A, Perez-Wurfl I and Barnett A 2015 Material and device analysis of SiGe solar cell in a GaAsP–SiGe dual junction solar cell on Si substrate *Solar Energy Mater. Solar Cells* **134** 114–21
[26] Wang L, Conrad B, Soeriyadi A and Diaz M 2015 Current matched GaAsP/SiGe tandem device on Si over 20% efficiency under indoor measurement *IEEE 42nd Photovoltaic Specialists Conf.* (IEEE) pp 1–4
[27] Li D, Zhao X, Diaz M, Conrad B and Wang L 2015 Optical and electrical analysis of graded buffer layers in III–V/SiGe on silicon tandem solar cells *IEEE 42nd Photovoltaic Specialist Conf.* (IEEE) pp 1–3
[28] Diaz M, Wang L, Gerger A and Lochtefeld A 2014 Dual-junction GaAsP/SiGe on silicon tandem solar cells *IEEE 40th Photovoltaic Specialists Conf.* (IEEE) pp 0827–30
[29] Grassman T J, Brenner M R, Rajagopalan S, Unocic R, Dehoff R, Mills M, Fraser H and Ringel S A 2009 Control and elimination of nucleation-related defects in GaP/Si(001) heteroepitaxy *Appl. Phys. Lett.* **94** 232106
[30] Grassman T J, Carlin J A, Galiana B, Yang L M, Yang F, Mills M J and Ringel S A 2013 Nucleation-related defect-free GaP/Si(100) heteroepitaxy via metal-organic chemical vapor deposition *Appl. Phys. Lett.* **102** 142102–5
[31] Vaisman M, Fan S, Nay Yaung K, Perl E, Martín-Martín D, Yu Z J, Leilaeioun M, Holman Z C and Lee M L 2017 15.3%-efficient GaAsP solar cells on GaP/Si templates *ACS Energy Lett.* **2** 1911–8
[32] Yaung K N, Vaisman M, Lang J and Lee M L 2016 GaAsP solar cells on GaP/Si with low threading dislocation density *Appl. Phys. Lett.* **109** 032107
[33] Chmielewski D J, Grassman T J, Carlin A M, Carlin J A, Speelman A J and Ringel S A 2014 Metamorphic GaAsP tunnel junctions for high-efficiency III–V multijunction solar cell technology *IEEE J. Photovolt.* **4** 1301–5
[34] Grassman T J, Chmielewski D J, Carnevale S D, Carlin J A and Ringel S A 2015 $GaAs_{0.75}P_{0.25}$/Si dual-junction solar cells grown by MBE and MOCVD *IEEE J. Photovolt.* **6** 326–31
[35] Dimroth F *et al* 2014 Comparison of direct growth and wafer bonding for the fabrication of GaInP/GaAs dual-junction solar cells on silicon *IEEE J. Photovolt.* **4** 620–5
[36] Tong Q Y, Schmidt E, Gösele U and Reiche M 1994 Hydrophobic silicon wafer bonding *Appl. Phys. Lett.* **64** 625–7
[37] Chung T R, Yang L, Hosoda N and Suga T 1997 Room temperature GaAs-Si and InP-Si wafer direct bonding by the surface activated bonding method *Nucl. Instrum. Methods Phys. Res.* B **121** 203–6
[38] Dai P, Lu S, Uchida S, Ji L, Wu Y, Tan M, Bian L and Yang H 2015 Room-temperature wafer bonded InGaP/GaAs//InGaAsP/InGaAs four-junction solar cell grown by all-solid state molecular beam epitaxy *Appl. Phys. Express* **9** 016501–5
[39] Dimroth F *et al* 2014 Wafer bonded four-junction GaInP/GaAs//GaInAsP/GaInAs concentrator solar cells with 44.7% efficiency *Prog. Photovolt., Res. Appl.* **22** 277–82
[40] Chiu P T *et al* 2013 Direct semiconductor bonded 5J cell for space and terrestrial applications *IEEE J. Photovolt.* **4** 493–7
[41] Liang J, Chai L, Nishida S, Morimoto M and Shigekawa N 2015 Investigation on the interface resistance of Si/GaAs heterojunctions fabricated by surface-activated bonding *Japan. J. Appl. Phys.* **54** 030211–6
[42] Derendorf K *et al* 2013 Fabrication of GaInP/GaAs//Si solar cells by surface activated direct wafer bonding *IEEE J. Photovolt.* **3** 1423–8

[43] Cariou R *et al* 2016 Monolithic two-terminal III–V//Si triple-junction solar cells with 30.2% efficiency under 1-sun AM1.5g *IEEE J. Photovolt.* **7** 367–73

[44] Cariou R, Benick J, Beutel P, Tucher N, Graf M and Lackner D 2017 Wafer bonded III–V on silicon multi-junction cell with efficiency beyond 31% *IEEE 44th Photovoltaic Specialists Conf. (Washington, DC)*

[45] Shigekawa N, Liang J, Onitsuka R, Agui T, Juso H and Takamoto T 2015 Current-voltage and spectral-response characteristics of surface-activated-bonding-based InGaP/GaAs/Si hybrid triple-junction cells *Japan. J. Appl. Phys.* **54** 08KE03–6

[46] Tanabe K, Watanabe K and Arakawa Y 2012 III–V/Si hybrid photonic devices by direct fusion bonding *Sci. Rep.* **2** 1–6

[47] Takamoto T, Ikeda E, Agui T, Kurita H, Tanabe T, Tanaka S, Matsubara H, Mine Y, Takagishi S and Yamaguchi M 1997 InGaP/GaAs and InGaAs mechanically-stacked triple-junction solar cells *Record 26th IEEE Photovoltaic Specialists Conf.* (IEEE) pp 1031–4

[48] Essig S, Ward S, Steiner M A, Friedman D J and Geisz J F 2015 Progress towards a 30% efficient GaInP/Si tandem solar cell *Energy Proc.* **77** 464–9

[49] Essig S *et al* 2016 Realization of GaInP/Si dual-junction solar cells with 29.8% 1-sun efficiency *IEEE J. Photovolt.* **6** 1012–9

[50] Essig S *et al* 2017 Raising the one-sun conversion efficiency of III–V/Si solar cells to 32.8% for two junctions and 35.9% for three junctions *Nat. Energy* **2** 17144

[51] Takamoto T, Washio H, Yamaguchi H, Ijichi R, Suzuki Y, Shimada K, Takahashi N and Oka S 2017 IMM triple-junction solar cells, module optimized for space and terrestrial conditions *IEEE 44th Photovoltaics Specialists Conf. (Washington, DC)*

[52] Yablonovitch E, Hwang D M, Gmitter T J, Florez L T and Harbison J P 1990 Van der Waals bonding of GaAs epitaxial liftoff films onto arbitrary substrates *Appl. Phys. Lett.* **56** 2419

[53] Mizuno H, Makita K and Matsubara K 2012 Electrical and optical interconnection for mechanically stacked multi-junction solar cells mediated by metal nanoparticle arrays *Appl. Phys. Lett.* **101** 191111–5

[54] Mizuno H, Makita K, Sugaya T, Oshima R, Hozumi Y, Takato H and Matsubara K 2016 Palladium nanoparticle array-mediated semiconductor bonding that enables high-efficiency multi-junction solar cells *Japan. J. Appl. Phys.* **55** 025001

[55] Mizuno H, Makita K and Tayagaki T 2016 A 'smart stack' triple-junction cell consisting of InGaP/GaAs and crystalline Si *IEEE 43rd Photovoltaic Specialist Conf.* pp 1923–5

[56] Yang J, Peng Z, Cheong D and Kleiman R 2014 Fabrication of high-efficiency III–V on silicon multijunction solar cells by direct metal interconnect *IEEE J. Photovolt.* **4** 1149–55

[57] Krogstrup P, Jørgensen H I, Heiss M, Demichel O, Holm J V, Aagesen M, Nygard J and Fontcuberta I Morral A 2013 Single-nanowire solar cells beyond the Shockley–Queisser limit *Nat. Photon.* **7** 306–10

[58] Heiss M, Russo-Averchi E, Dalmau-Mallorquí A, Tütüncüoğlu G, Matteini F, Rüffer D, Conesa-Boj S, Demichel O, Alarcón-Lladó E and Fontcuberta I Morral A 2013 III–V nanowire arrays: growth and light interaction *Nanotechnology* **25** 014015

[59] Gudiksen M S, Lauhon L J, Wang J, Smith D C and Lieber C M 2002 Growth of nanowire superlattice structures for nanoscale photonics and electronics *Nature* **415** 415617a–620

[60] Otnes G and Borgström M T 2017 Towards high efficiency nanowire solar cells *Nano Today* **12** 31–45

[61] Aberg I *et al* 2015 A GaAs nanowire array solar cell with 15.3% efficiency at 1 sun *IEEE J. Photovolt.* **6** 185–90

[62] Bocquillon E, Freulon V, Berroir J M, Degiovanni P, Placais B, Cavanna A, Jin Y and Feve G 2013 Coherence and indistinguishability of single electrons emitted by independent sources *Science* **339** 1054–7

[63] Sburlan S, Daniel Dapkus P and Nakano A 2012 Critical dimensions of highly lattice mismatched semiconductor nanowires grown in strain-releasing configurations *Appl. Phys. Lett.* **100** 163108

[64] Glas F 2006 Critical dimensions for the plastic relaxation of strained axial heterostructures in free-standing nanowires *Phys. Rev.* B **74** 208

[65] Chuang L C, Moewe M, Chase C, Kobayashi N P, Chang-Hasnain C and Crankshaw S 2007 Critical diameter for III–V nanowires grown on lattice-mismatched substrates *Appl. Phys. Lett.* **90** 043115

[66] Ertekin E, Greaney P A, Chrzan D C and Sands T D 2005 Equilibrium limits of coherency in strained nanowire heterostructures *J. Appl. Phys.* **97** 114325

[67] Kandala A, Betti T and Fontcuberta I Morral A 2009 General theoretical considerations on nanowire solar cell designs *Phys. Status Solidi* a **206** 173–8

[68] Yao M, Cong S, Arab S, Huang N, Povinelli M L, Cronin S B, Dapkus P D and Zhou C 2015 Tandem solar cells using GaAs nanowires on Si: design, fabrication, and observation of voltage addition *Nano Lett.* **15** 7217–24

[69] Beltz G E, Chang M, Eardley M A, Pompe W, Romanov A E and Speck J S 1997 A theoretical model for threading dislocation reduction during selective area growth *Mater. Sci. Eng.* A **234–6** 794–7

[70] Lee S C, Dawson L R, Brueck S R J and Jiang Y B 2005 GaAs on Si(1 1 1)-crystal shape and strain relaxation in nanoscale patterned growth *Appl. Phys. Lett.* **87** 023101

[71] Taboada A G *et al* 2014 Strain relaxation of GaAs/Ge crystals on patterned Si substrates *Appl. Phys. Lett.* **104** 022112–6

[72] Chu C-P *et al* 2014 Nanoscale growth of GaAs on patterned Si(1 1 1) substrates by molecular beam epitaxy *Cryst. Growth Des.* **14** 593–8

[73] Hsu C-W, Chen Y-F and Su Y-K 2012 Nanoepitaxy of GaAs on a Si(0 0 1) substrate using a round-hole nanopatterned SiO 2mask *Nanotechnology* **23** 495306–7

[74] Warren E L, Makoutz E A, Horowitz K A W, Dameron A, Norman A G, Stradins P, Zimmerman J D and Tamboli A C 2016 Selective area growth of GaAs on Si patterned using nanoimprint lithography *IEEE 43rd Photovoltaic Specialists Conf.* pp 1938–41

[75] Greenaway A L, Sharps M C, Boucher J W, Strange L E, Kast M G, Aloni S and Boettcher S W 2016 Selective area epitaxy of GaAs microstructures by close-spaced vapor transport for solar energy conversion applications *ACS Energy Lett.* **1** 402–8

[76] Essig S and Dimroth F 2013 Fast atom beam activated wafer bonds between n-Si and n-GaAs with low resistance *ECS J. Solid State Sci. Technol.* **2** Q178–81

[77] Brandt R E *et al* 2017 Searching for 'defect-tolerant' photovoltaic materials: combined theoretical and experimental screening *Chem. Mater.* **29** 4667–74

[78] Noh J, Im S, Heo J, Mandal T and Seok S 2013 Chemical management for colorful, efficient, and stable inorganic organic hybrid nanostructured solar cells *Nano Lett.* **13** 1764–9

[79] Yang W S, Noh J H, Jeon N J, Kim Y C, Ryu S, Seo J and Seok S I 2015 High-performance photovoltaic perovskite layers fabricated through intramolecular exchange *Science* **348** 1234–7

[80] Park N 2014 Perovskite solar cells: an emerging photovoltaic technology *Mater. Today* **18** 65–72

[81] Yang S, Fu W, Zhang Z, Chen H and Li C 2017 Recent advances in perovskite solar cells: efficiency, stability and lead-free perovskite *J. Mater. Chem.* A **5** 11462
[82] Correa Baena J P, Abate A, Saliba M, Tress W, Jacobsson T J, Grätzel M and Hagfeldt A 2017 The rapid evolution of highly efficient perovskite solar cells *Energy Environ. Sci.* **10** 710–27
[83] Bush K A *et al* 2017 23.6%-efficient monolithic perovskite/silicon tandem solar cells with improved stability *Nat. Energy* **2** 17009
[84] Filipič M, Löper P, Niesen B, De Wolf S, Krč J, Ballif C and Topič M 2015 CH3NH3PbI3 perovskite/silicon tandem solar cells: characterization based optical simulations *Opt. Express* **23** A263
[85] Foster S and John S 2016 Light-trapping design for thin-film silicon-perovskite tandem solar cells *J. Appl. Phys.* **120** 103103
[86] Loper P, Moon S-J, Nicolas S M D, Niesen B, Ledinsky M, Nicolay S, Bailat J, Yum J-H, De Wolf S and Ballif C 2014 Organic-inorganic halide perovskite/crystalline silicon four-terminal tandem solar cells *Phys. Chem. Chem. Phys.* **17** 1619–29
[87] Bailie C D *et al* 2015 Semi-transparent perovskite solar cells for tandems with silicon and CIGS *Energy Environ. Sci.* **8** 956–63
[88] Mailoa J P, Bailie C D, Johlin E C, Hoke E T, Akey A J, Nguyen W H, McGehee M D and Buonassisi T 2015 A 2-terminal perovskite/silicon multijunction solar cell enabled by a silicon tunnel junction *Appl. Phys. Lett.* **106** 121105
[89] Albrecht S *et al* 2015 Monolithic perovskite/silicon-heterojunction tandem solar cells processed at low temperature *Energy Environ. Sci.* **9** 81–8
[90] Werner J, Weng C-H, Walter A, Fesquet L, Seif J P, De Wolf S, Niesen B and Ballif C 2016 Efficient monolithic perovskite/silicon tandem solar cell with cell area $> 1\,\mathrm{cm}^2$ *J. Phys. Chem. Lett.* **7** 161–6
[91] McMeekin D P *et al* 2016 A mixed-cation lead mixed-halide perovskite absorber for tandem solar cells *Science* **351** 151–5
[92] Chen B *et al* 2016 Efficient semitransparent perovskite solar cells for 23.0%-efficiency perovskite/silicon four-terminal tandem cells *Adv. Energy Mater.* **6** 1601128
[93] Werner J *et al* 2016 Efficient near-infrared-transparent perovskite solar cells enabling direct comparison of 4-terminal and monolithic perovskite/silicon tandem cells *ACS Energy Lett.* **1** 474–80
[94] Tamboli A C, Bobela D C, Kanevce A, Remo T, Alberi K and Woodhouse M 2017 Low-cost CdTe/silicon tandem solar cells *IEEE J. Photovolt.* **7** 1767–72
[95] Carmody M, Mallick S, Margetis J, Kodama R, Biegala T, Xu D, Bechmann P, Garland J W and Sivananthan S 2010 Single-crystal II–VI on Si single-junction and tandem solar cells *Appl. Phys. Lett.* **96** 153502
[96] Rau U 2007 Reciprocity relation between photovoltaic quantum efficiency and electroluminescent emission of solar cells *Phys. Rev.* B **76** 085303–8
[97] Yao J *et al* 2015 Quantifying losses in open-circuit voltage in solution-processable solar cells *Phys. Rev. Appl.* **4** 014020–10
[98] Green M A 2011 Radiative efficiency of state-of-the-art photovoltaic cells *Prog. Photovolt., Res. Appl.* **20** 472–6
[99] Green M A 1982 *Solar Cells: Operating Principles, Technology and System Applications* (*Prentice-Hall Series in Solid State Physical Electronics*) (Kensington: Prentice-Hall)
[100] Yamaguchi M, Yamada H, Katsumata Y, Lee K-H, Araki K and Kojima N 2017 Efficiency potential and recent activities of high-efficiency solar cells *J. Mater. Res.* **32** 3445–57